The Anomalous Mole Fraction Effect in *Chara*: Gating at the Edge of Temporal Resolution

Afshin Farokhi, Maike Keunecke, and Ulf-Peter Hansen
Center of Biochemistry and Molecular Biology, 24098 Kiel, Germany

ABSTRACT The anomalous mole fraction effect (AMFE) of the K^+ channel in excised patches of the tonoplast of *Chara* showed a minimum of apparent open-channel current at 20 mM Tl^+ and 230 mM K^+. Time series obtained at a sampling rate of 100 kHz (filter 25 kHz) were analyzed by three methods to find out whether the AMFE results from an effect on gating or on the conductivity of the open state. Fitting the amplitude histograms by a superposition of gaussians showed a broadening in the presence of Tl^+. Dwell-time analysis based on an O–O–C–C–C model failed to evaluate rate constants above the filter frequency. Thus, the absence of any reduction of apparent open-channel current in time series simulated with the evaluated rate constants could not be taken as evidence against the hypothesis of gating. Finally, a direct fit of the measured time series using five different 5-state Hidden Markov models revealed that the presence of Tl^+ changed the rate constants in such a way that the number of transitions into the short-lived open state (30 μs) increased strongly compared to those in the absence of Tl^+. These models explain 25% reduction of apparent single-channel current amplitude through a rapid gating mechanism.

INTRODUCTION

The anomalous mole fraction effect (AMFE) describes the peculiar finding that the current in a mixture of certain ions is found to be smaller than in the pure solutions. This occurs in solutions of Tl^+/K^+ in plant channels (Tester, 1988; Draber et al., 1991) or in animal channels (Hagiwara et al., 1977; Wagoner and Oxford, 1987), in solutions of K^+/Rb^+ or $NH_4{}^+/Rb^+$ (Eisenman et al., 1986), in the Ca^{2+} channel (Ca^{2+}/Ba^{2+}: Friel and Tsien, 1989; Hess and Tsien, 1984), or in the Cl^- channel (Cl^-/SCN^-: Dietrich and Hedrich, 1998; Tabcharani et al., 1993).

Different theories of channel transport have tried to explain the AMFE. Especially, the AMFE was believed to be a stronghold of the Hille–Schwarz model (Hille and Schwarz, 1978) with two binding sites in the channel. The electrostatic repulsion force of a second ion is necessary to free an ion from the binding site. This model, adopted by many workers (e.g., Ciani et al., 1978), got strong support from different findings; e.g., For instance, Baukrowitz and Yellen (1996) showed that the probability of leaving the channel decreased dramatically when no second ion was available. Tabcharani et al. (1993) found that changing the positive charge of Arg-347 on a channel helix to a negative one (Asp) abolished the AMFE.

Nevertheless, even though Doyle et al. (1998) showed the existence of at least two binding sites in the KcsA channel, the necessity of the multi-site assumption for the AMFE may be questioned. Pietrobon et al. (1988) suggested that conformational changes of the dihydropyridine-sensitive (L-type) Ca^{2+} channel induced by a permeating ion can be felt by a subsequent one, as concluded from the observation of the destabilization of a protonated state of a group on the external channel surface by the permeating cation. Also Pallotta and Wagoner (1992) discussed the problem of permeation models and made the statement that the multi-site model is a problem.

Alternative models, avoiding the assumption of a multi-site channel, were suggested by Wu (1991, 1992) and by Nonner et al. (1998). In the Wu model, the kinetic energy of the approaching second ion is necessary to free the ion from the single binding site. Similar to the Hille–Schwarz model, the mutual liberation from the binding site works best if both ions are equal. Nonner et al. (1998) showed that even a mean-field theory like Poisson–Nernst–Planck, not based on discrete structures like channels, could create an AMFE.

However, there is one question that is even more basic than the above models: Is the AMFE a permeation or a gating effect (Hansen et al., 1997; Townsend and Horn, 1999)? In the case of a permeation effect, the average time between the passage of two ions (conductivity of the open state) is influenced. Alternatively, a gating mechanism would keep the average distance between permeating ions constant, but the stream of ions is interrupted by periods of inactivity. This gating may remain undetected if the temporal resolution of the recording set-up is not sufficient for resolving the interruptions of ion flux.

The involvement of a gating effect was shown to be the cause when apparent open-channel conductivity was reduced during Cs^+ block (Draber and Hansen, 1994). In records with a sampling rate of 5 kHz, a negative slope of the IV-curve occurred at negative membrane voltages in the presence of 5 to 25 mM Cs^+. This reduction in open-channel current was not found when the sampling rate was 100 kHz. The above considerations and the findings in the case of the Cs^+ led to the question of whether fast gating also plays a crucial rule in the AMFE.

Received for publication 13 July 2000 and in final form 14 September 2000.

Address reprint requests to Ulf-Peter Hansen, Center of Biochemistry and Molecular Biology (ZBM), Leibnizstr. 11, 24098 Kiel, Germany. Tel.: +49-431-880-3960/61; Fax: +49-431-880-3943; E-mail: ulf@bio-physik.uni-kiel.de.

0006-3495/00/12/3072/11 $2.00

MATERIALS AND METHODS

Tonoplast vesicles of *Chara*

Chara corallina Klein ex Willd., a gift of D. Gradmann (Biophysik der Pflanzen, Göttingen, Germany) was grown in the lab in plastic basins filled with artificial pond water (0.1 mM $CaCl_2$, 0.1 mM NaCl, 1.0 mM KCl) on a layer of rotten beech-tree leaves and sand. Patch clamp experiments were done on excised patches (inside-out) of cytoplasmic droplets. According to Lühring (1986) and Sakano and Tazawa (1986), the membrane is a tonoplast (surrounding the vacuole). After wilting, cells of *Chara* were cut, and the cytosol formed droplets at the bottom of the experimental vessel in a solution of 250 mM KNO_3 and 5 mM $Ca(NO_3)_2$. NO_3^- rather than Cl^- was used as anion to allow the replacement of K^+ by Tl^+. Sealing, however, seemed to work less well in NO_3^- than in Cl^-.

Electrophysiology

The experimental set-up is described in detail by Draber and Hansen (1994). The vessel with the bathing fluid was modified to enable rapid exchange of the medium.

Electrodes were made from borosilicate glass (Hilgenberg, Malsfeld, Germany), coated internally with Sigmacote (Sigma, Deisenhofen, Germany), drawn on an L/M-3P-A puller (List, Darmstadt, Germany), fire-polished, and filled with 250 mM KNO_3 + 5 mM $Ca(NO_3)_2$. This solution was also used for the bathing medium if not otherwise mentioned. Externally, coating with Sylgard (Dow Corning, Midland, MI) was not used because this hindered the operation of the patch close to the surface of the bath (Fig. 1). Patch clamp current was recorded by a List EPC 7 (List) with the internal low-pass filters being switched off. Data was stored on disk with a sampling rate of 100 kHz. The four-pole Bessel anti-aliasing filter was set to 25 kHz. The sign of membrane potential corresponds to the convention: luminal side (pipette in inside-out patches) is zero.

The signal-to-noise ratio is crucial for temporal resolution. The dominant source of noise arises from pipette capacitance (Sigworth, 1983) of that part wetted by the bath solution after the coating procedures described above had been applied. Noise could be reduced by a factor of 2.2 ($\pm$ 0.5) when the pipette with the excised patch (inside-out) was kept close to the surface of the solution (20 μm, Fig. 1). In these experiments, the Dagan 3900A amplifier (Dagan, Minneapolis, MN) was used with a four-pole anti-aliasing filter of 50 kHz.

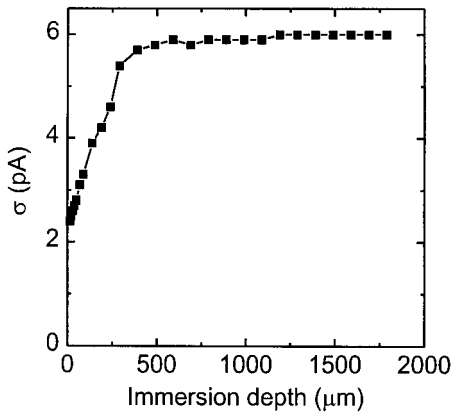

FIGURE 1 Dependence of current noise (σ) on the length of the pipette tip in contact with the bath solution. Excised patch with a seal resistance of 5 GΩ. Sampling rate; 200 kHz, Bessel filter: 50 kHz.

Data analysis

Open-channel currents were determined from fitting the amplitude histograms by a sum of gaussians (Eq. 5) and controlled by visual positioning lines in the middle of the levels of the time series on the computer screen. Both methods led to the same results. The analysis of gating was done with the lab-made programme day.pas using a fourth-order Hinkley detector for jump detection (Schultze and Draber, 1993; Hansen et al., 1995).

Multi-channel multi-state dwell-time analysis (Blunck et al., 1998) was done by means of merging the individual channels to a macro-channel. In the case of a two-channel five-state model (A–O–G–C–Z, with A and O being open and G, C, and Z closed states), the 25 states of the macro-channel are generated by all combinations of two channels $\{S_1, S_2\}$ with S_1 and S_2 being A, O, G, C, or Z. The transition rates of the macro-channel κ_{rs} are calculated from the transition rates k_{ij} of the single-channel model

$$\kappa_{rs} = b_i^{(r)} \cdot k_{ij} \tag{1}$$

with $b_I^{(r)}$ being the component of a vector that describes whether transitions from macro-state r with the single-channel rate constants k_{ij} are possible or not.

The p.d.f. $y_m(t)$ for the dwell times in the current level Y_m is

$$y_m(t) = \sum_{i=1}^{B_m} d_i^{(m)} \exp(-\lambda_i^{(m)} t) \tag{2}$$

$$d_i^{(m)} = 2S_m \sum_{r \in Y_m} R_r^{(m)}(\infty) v_r^{(m,i)} \cdot \left(\sum_{r \in Y_m} \sum_{s \notin Y_m} \kappa_{rs} \right)^2 \Big/ f_{tr}^{(m)}, \tag{3}$$

with m = index of the macro-state level, r and s = indices of the macro states, d_i = amplitude factors, $\lambda_i^{(m)}$ = eigenvalues, $v_r^{(m,i)}$ = eigenvectors of the transition matrix, $R_r^{(m)}$ = steady-state occupation, S_m = scaling factor, $f_{tr}^{(m)}$ = average transition frequency of the macro state level m. Alternatively, the kinetic behavior was analyzed by a direct fit of the time series making use of the one-step prediction algorithm suggested by Baum et al. (1970). These equations were used by Chung et al. (1990) and Chung and Gage (1998) for the restoration and identification of the conductance levels. They estimated the transition probabilities p_{ij} by means of the Baum–Welch algorithm. However, to estimate the rate constants of the state transitions, k_{ij}, Fredkin and Rice (1992) used only the forward prediction step. This approach was extended by Albertsen and Hansen (1994) for multi-state multi-channel analysis.

The forward prediction step gives the forward variable in the Baum–Welch algorithm,

$$a_k(s) = \sum_r a_{k-1}(r) p_{rs} f_S(y_k), \tag{4}$$

where $a_k(s)$ is the probability that the macro channel is in state s at time k with the macro-channel states being r, s = {AA, AO, AG, AC, AZ, OA, etc} as in the dwell-time analysis above, p_{rs} is the transition probability calculated for the sampling interval Δt from the macro-channel rate constants κ_{rs}. For short Δt, $p_{rs} = \kappa_{rs}\Delta t$, otherwise an exponential function is involved (Albertsen and Hansen, 1994). f_S is a partial amplitude histogram giving the probability that state s (belonging to those macro states s that cause the same current Y_S) of the Markov model can generate the current y_k measured at time k. Here, f_S is obtained by fitting the measured amplitude histogram $f(y_k)$ by a sum of gaussians,

$$f(y_k) = \sum_s f_S(y_k) = \sum_s c_S \exp\left(-\frac{(Y_S - y_k)^2}{\sigma^2} \right), \tag{5}$$

where σ is equal for all levels Y_s if it originates from superimposed noise.

The likelihood L obtained from the whole time series is

$$L = \prod_{k=1}^{N} \sum_{r} \sum_{s} a_{k-1}(r) p_{RS} f_S(y_k). \quad (6)$$

The highest value of L is obtained when the measured current y_k is assigned with the highest probability ($f_S(y_k)$) to that state which is predicted by the term ($a_{k-1}(r)\ p_{rs}$) with the highest probability. A downhill simplex algorithm (Press et al., 1987) is used to find that set of single-channel rate constants k_{ij} that give the maximum likelihood. Even though p_{rs} is used in Eq. 6, the single-channel rate constants k_{ij} are evaluated, because, in each iteration step of the fit routine, the simplex algorithm suggests a set of k_{ij} of the individual channel, and the κ_{rs} and p_{rs} are calculated by means of Eq. 1 (Blunck et al., 1998) and the Kolmogorov equation $P = \exp(K\Delta t)$ (Albertsen and Hansen, 1994) with P and K being the matrices of p_{rs} and κ_{rs}, respectively.

Simulations

Simulations of time series for Hidden-Markov Models were performed by the algorithm of Riessner (1998) described by Blunck et al. (1998). Two random generators were used; one for the determination of the time of the jump (depending on the rate constant) and one for the sink state of the jump. The effect of the anti-aliasing filter was introduced as follows: the response of a four-pole Bessel filter with a corner frequency of 25 kHz was stored in the computer. Whenever the random generator caused a jump, the filter response was taken from the memory and added to the existing time course. Noise was superimposed by taking values from a stored noise record with the same anti-aliasing filter. The signal-to-noise ratio was $I/\sigma = 2.2$. The single-channel current i_{sim} was the current used in the simulations. The apparent open-channel current of the simulated time series (i_{fit}) was determined by the same procedure as in the case of the apparent single-channel current of the measured time series, i.e., fitting the amplitude histograms by a sum of gaussians (Eq. 5) controlled by visual inspection.

RESULTS AND DISCUSSION

The AMFE in the apparent open-channel current

Figure 2 shows the AMFE effect. Records in solutions of different Tl^+/K^+ ratios show that the minimum of apparent current occurs ~5–10 mM Tl^+. The experiments of Fig. 2 were done with $[TlNO_3] + [KNO_3] = 150$ mM and 5 mM $Ca(NO_3)_2$ (Fig. 2). Figure 3 shows that the total cation concentration is not crucial for the occurrence of the AMFE, it is observed also at $[TlNO_3] + [KNO_3] = 250$ mM. The AMFE is asymmetric with respect to membrane potential. With Tl^+ in the bath, the AMFE occurs at positive potentials (in the bath). This implies that an AMFE is obtained when the current drags Tl^+ ions into the pore (*open circles* in Fig. 3). An AMFE at positive and negative voltages is obtained only if Tl^+ is on both sides of the membrane (*crosses* in Fig. 3). This is in contrast to previous measurements of Keunecke (Hansen et al., 1997) and probably also to the measurements of Draber et al. (1991) on the same channel. The reasons for these symmetric effects are unknown because they have not been observed in other than these early studies.

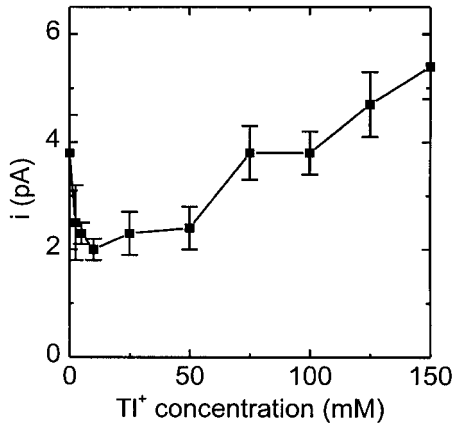

FIGURE 2 Dependence of apparent single open-channel channel current in inside-out patches of *Chara* droplets on Tl^+ concentration ($[Tl^+] + [K^+] = 150$ mM). Membrane voltage was +80 mV (bath = cytosolic side). The error bars show standard deviations derived from 4 to 7 experiments.

The AMFE: gating or permeation?

Time series and amplitude histograms

The following experiments were done at a total concentration of $[Tl^+] + [K^+] = 250$ mM and $[Ca^{2+}] = 5$ mM, as in Fig. 3. The higher total concentration (as compared to Fig. 2) turned out to be useful to improve the signal-to-noise ratio (higher single-channel currents), which is crucial for the temporal resolution. Figure 4 shows two records of patch clamp current obtained from an excised membrane (inside-out) with 2 channels at a sampling rate of 100 kHz and a four-pole anti-aliasing filter of 25 kHz.

At a time scale in the range of seconds, the current levels can be easily identified in the record in 250 mM KNO_3 (Fig.

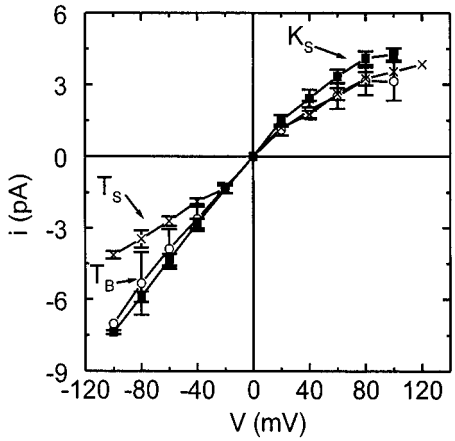

FIGURE 3 Sideness of the AMFE. IV-curves measured in $[Tl^+] + [K^+] = 250$ mM and 5 mM $Ca(NO_3)_2$ at room temperature in symmetrical K^+ solution (K_s, *filled squares*), with asymmetrical Tl^+ solution (20 mM Tl^+ in the bathing medium = cytosolic side, T_B, *open circles*) and symmetrical Tl^+ solution (20 mM Tl^+ on either side, T_s, *crosses*).

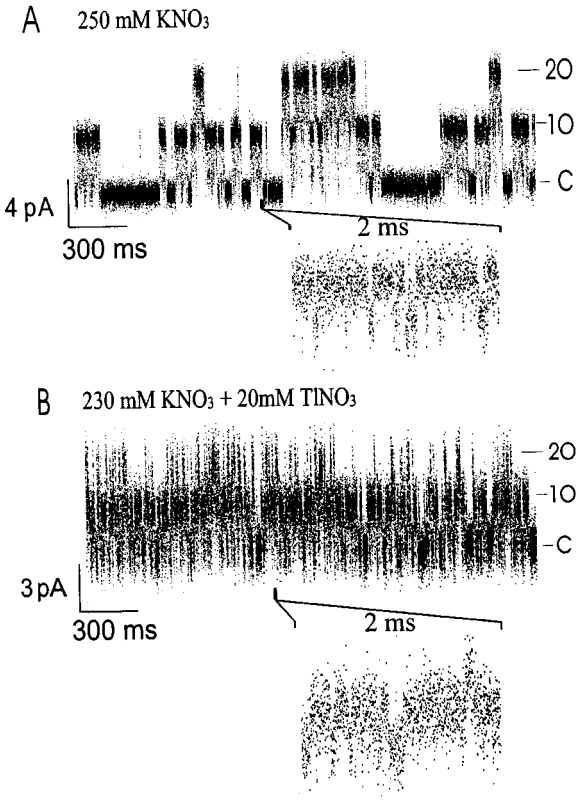

FIGURE 4 Current traces (250,000 data points) obtained from vesicles of *Chara* in (*A*) 250 mM KNO_3 + 5 mM $Ca(NO_3)_2$ and in (*B*) 230 mM KNO_3 + 20 mM $TlNO_3$ + 5 mM $Ca(NO_3)_2$. C, 1O, and 2O at the right-hand side give the current levels (C = closed, 1O = 1 channel open, 2O = two channels open). Membrane voltage was +100 mV. The length of the expanded sections is 2 ms.

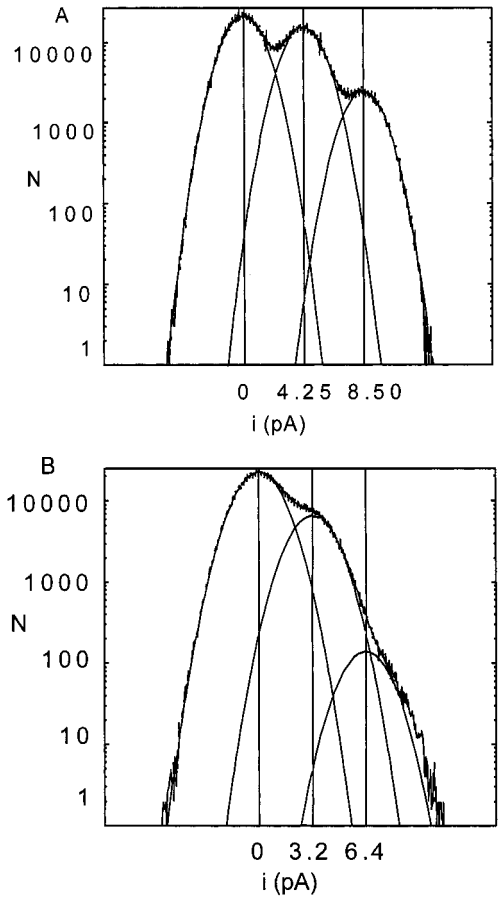

FIGURE 5 Amplitude histograms obtained from time series measured at +100 mV in (*A*) 250 mM KNO_3 + 5 mM $Ca(NO_3)_2$ and in (*B*) 230 mM KNO_3 + 20 mM $TlNO_3$ + 5 mM $Ca(NO_3)_2$. Data is taken from different patches. Sampling rate was 100 kHz with four-pole Bessel filter, 25 kHz, $2 \cdot 10^6$ samples. N = frequency per bin (0.06 pA). Smooth lines give the fit by a sum of gaussians and the partial amplitude histograms per level. σ was (A)1.3 pA and (B) 1.7 pA. A significant difference between the σ of open and closed levels was not found.

4 *A*). In the presence of Tl^+, the records become more "noisy," however it can be easily imagined that a filter in the range of 1 kHz would reveal clear current levels. The problem of the analysis of fast gating gets obvious when the current traces are displayed on an expanded time scale (insets of 2-ms sections in Fig. 4, *A* and *B*). These expanded parts (which show each one of the data points at a sampling rate of 100 kHz) illustrate the problems that have to be overcome if the single-channel current is to be determined from channels with fast gating.

The standard approach is the generation of amplitude histograms like those in Fig. 5, and fitting them by a sum of gaussians to obtain the apparent single-channel current (Eq. 5). If fast gating (rate constants higher than the cutoff frequency of the filter) is involved, the gaussians may be converted to β distributions (FitzHugh, 1983; Yellen 1984). In extreme cases, the involvement of β distributions becomes obvious by strong deviations of the curve shape from that of gaussians (asymmetry). For instance, they were used by Klieber and Gradmann (1993) for the detection of the involvement of fast gating in the Cs^+ block before Draber and Hansen (1994) could reveal the fast rate constants directly.

However, fast gating not so far beyond the filter frequency would result in broadening of the gaussians without visible deviation from the typical shape. Such an effect is indicated in Fig. 5. The amplitude histograms without and with Tl^+ can be fitted by gaussians, but they are broader for the Tl^+ data (Fig. 5 *B*). This broadening affects not only the current variance σ of the open channel, but also that of the closed-level (because the dwell time in the closed level is also very short during fast flickering), as can be seen from the baseline in Fig. 4 *B* (and as will become obvious in Table 3, below). The broadening (σ = 1.3 pA without and σ = 1.7 pA with Tl^+ in Fig. 5) suggests that fast gating is the cause of the reduction of single-channel current in Figs. 2–5.

Testing the hypothesis that the AMFE is a gating effect

The strategy

There is no simple theory that describes how the filter of the recording apparatus changes the true single-channel current to the apparent single-channel obtained from the evaluation of the amplitude histogram. For this purpose, the theory of β distributions had to be extended to multi-channel multi-state records, which is available only for first-order filters (Riessner, 1998). Thus, simulations have to be used. A Markov model that has been shown to yield the same kinetic behavior as the biological channel is used to generate a time series. This time series is superimposed by the same noise as found in the experiments. Then, the resulting record is analyzed by the same method as used for the real data to determine the apparent single-channel current. Because, in a simulation, the "true" single-channel current (i_{sim}) is known, the effect of filtering on the apparent single-channel current (i_{fit}) can be obtained in quantitative terms from the comparison with the true current.

A more difficult problem is how to get the Markov model of the real channel and its rate constants. Fortunately, for this issue, it is not necessary to find the true model. It is sufficient to find one that creates time series that have the same kinetic properties as those of the biological channel, even though it would be a welcome fringe benefit if the selected model came close to the true one of the channel. Below, it is shown that the commonly used dwell-time analysis (Blunck et al., 1998) fails in the case of the Tl^+ data. However, the direct fit of the time series (Fredkin and Rice, 1992; Albertsen and Hansen, 1994; Klein et al., 1997) is sufficient for the task.

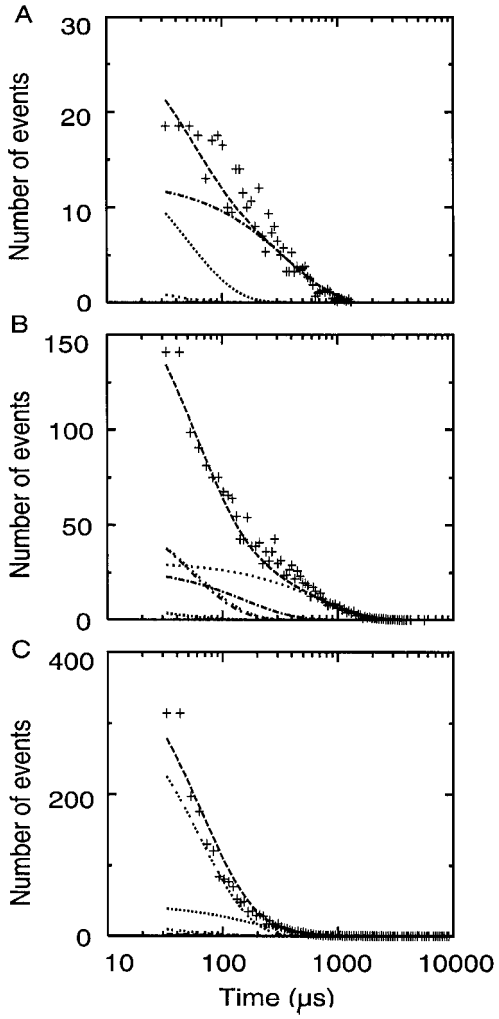

FIGURE 6 Multi-channel target fit of a 2-channel record (20 s, $2 \cdot 10^6$ data points) fitted with the A–O–G–C–Z model showing (*A*) level 2, (*B*) level 1, and (*C*) level 0. The smooth lines below the data give the individual exponentials of Eq. 2. The logarithmic time scale does not imply that the histogram is log-binned. The unit at the *y* axis is events/40 μs for all data points, even though averaging was done in exponentially increasing intervals.

An attempt to obtain the Markov model of the K^+ channel in *Chara* from a multi-channel multi-state dwell-time analysis

Evaluation of the rate constants

The "noise-free" time series were reconstructed from the measured records by means of a fourth-order Hinkley detector (Schultze and Draber, 1993; Hansen et al., 1995) whose temporal resolution of 20–60 μs (K^+) and 70–140 μs (Tl^+/K^+) was automatically selected according to a signal-to-noise ratio of i/σ = 3.5–2.4 (K^+) and 2.2–1.5 (Tl^+/K^+). Then, multi-channel dwell-time histograms were created.

Below, it is shown that four 5-state models were kinetically equivalent. One of those models, the linear A–O–G–C–Z model (A and O being open states with the same conductance, and G, C, and Z closed states) was used for a target fit of the multi-channel dwell-time histograms (Fig. 6). A target fit (Blunck et al., 1998) based on Eqs. 1–3 was used because it directly yields the rate constants of the selected Markov model. Fits with models with less than five states did not approximate the data points. The smooth lines in Fig. 6 beyond the data points are the individual exponentials of Eq. 2. Their numbers (3 for level 2, 6 for level 1, and 6 for level 0, partially not visible because the components coincide or the amplitude factors are very small) are higher than those expected for a one-channel record of a five-state model. This indicates that the relationship between time-constants and rate-constants of the Markov model is quite complex in multi-channel analysis. This is the reason that the amplitude factors and time constants of these individual components are not shown. Instead, Table 1 shows the averaged rate constants of the A–O–G–C–Z model as obtained from fitting 7 and 4 experimental dwell-time histograms without and with Tl^+, respectively.

TABLE 1 Averaged rate constants from 4 and 7 experiments on different patches recorded at 80–100 mV in the absence and presence of 20 mM Tl^+ as obtained from dwell-time analysis by means of Eqs. 1 to 3

Rate Constant	K^+ Solution	$K^+ + Tl^+$ Solution
K_{AO}	8,100 ± 3100	7,400 ± 3400
K_{OA}	10,000 ± 2300	11,000 ± 4700
K_{OG}	6,000 ± 3400	7,100 ± 4000
K_{GO}	9,200 ± 2200	7,500 ± 3300
K_{GC}	5,400 ± 3300	5,800 ± 3300
K_{CG}	1,700 ± 1200	2,400 ± 1300
K_{CZ}	2,300 ± 1300	1,700 ± 900
K_{ZC}	300 ± 200	300 ± 200
i_{fit}/i_{sim}	1.00 ± 0.00	1.00 ± 0.00

The upper eight rows show mean values ± SD. The last row presents the reduction of open-channel current i_{fit}/i_{sim} in a time series simulated with the average values of the rate constants and an open-channel current i_{sim}.

Generating time series from the evaluated rate constants

The influence of gating on apparent single-channel current was investigated by means of simulations. The averaged Tl^+ data in Table 1 were used to simulate the time series of the channel as described in the Materials and Methods section. Open-channel current (i_{sim}) was set to 4.5 pA for K^+ and for Tl^+/K^+ superimposed by noise of 1.3 pA and filtered with a four-pole Bessel filter (25 kHz as used in the experiments). Amplitude histograms obtained from the simulated time series were fitted by a sum of gaussians (Eq. 5) to determine the apparent open-channel currents i_{fit}. The last row in Table 1 gives the reduction i_{fit}/i_{sim} resulting from gating. According to this kind of analysis, Tl^+-induced gating seems to cause no reduction of apparent open-channel current.

Pitfalls of the dwell-time analysis

The dwell-time analysis may suffer from many restrictions (Blunck et al., 1998). A major concern is the need for a jump detector for the reconstruction of the noise-free time series. It is the origin of the missed-events problem (Roux and Sauvé, 1985; Yeo et al., 1988; Draber and Schultze, 1994; Colquhoun et al., 1996). Thus, it cannot be excluded that the true rate constants of the real channel were much faster than those evaluated by the dwell-time fit. This does occur as shown by the following simulations based on the averaged Tl^+-data of Table 1. To study the effect of missed-events, simulations as described in Materials and Methods were used to generate time series with different values of the fast rate constants of the direct open–close transitions, k_{GO} and k_{OG}. For this purpose, the values of k_{GO} and k_{OG} in Table 1 were changed by a common factor (to keep the steady-state occupancies) of 0.5–40. The time series obtained by these simulations were subject to the same dwell-time analysis as the measured time series. The rate-constants obtained from this analysis (k_{fit}) were compared with those used for the simulations (k_{sim}).

Figure 7 illustrates the problems of dwell-time analysis. For short time constants, there is a nice coincidence with the ($k_{fit} = k_{sim}$)-line. Correct values of the rate constants were detected up to those values obtained from the measured data (*box* in Fig. 7). However, higher simulated rate constants did not cause any increase of the evaluated ones. The ratio between k_{GO} and k_{OG} (*parallel horizontal lines* in Fig. 7) stays constant because the ratios are related to the occupancies of the states that can be determined with higher reliability than the absolute values of the rate constants. The flatness of the curves in Fig. 7 has a second message: it does not make sense to use retrospective missed-events corrections (Crouzy and Sigworth, 1990; Draber and Schultze, 1994), because the correction algorithms would start from identical values for all real rate constants higher than the resolution limit.

Dwell-time analysis failed also for alternative models. Because of this, further computations based on dwell-time analysis are not reported. Instead, further analysis was based on the more efficient direct fit of the time series.

Evaluating the rate constants from a direct fit of the experimental time series

Overcoming the limitations of the dwell-time fit

An approach that is less vulnerable to the missed-events problem (Draber and Schultze, 1994) is the direct fit of the time series as described by Eqs. 4–6. Unfortunately, the direct fit of a 20-s record ($2 \cdot 10^6$ data points) required 3 days on a 300-MHz Pentium II for a single time series with

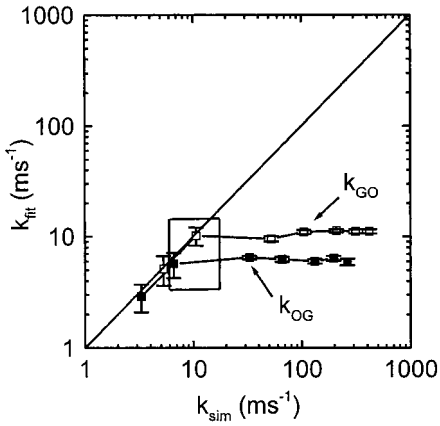

FIGURE 7 Testing the temporal resolution of the dwell-time analysis. The simulations of time series (20 s, $2 \cdot 10^6$ data points) were based on the average data in Table 1, but k_{GO} and k_{OG} were changed by a common factor of 0.5–40. k_{sim} at the abscissa gives the values of k_{GO} and k_{OG} used for the simulation of the time series. k_{fit} are the values of k_{GO} and k_{OG} obtained from the dwell-time analysis (Eqs. 1–3) of the simulated data. The box indicates the values obtained from the measured time series.

an O–O–C–C–C model and two channels. This reduced the number of suitable records to those four discussed below.

In a first set of computations, different five-state models were used. Table 2 shows the results obtained from the analysis of a two-channel record measured at +80 mV. The four linear models and one branched model resulted in about equal likelihoods. Even though the difference between the likelihoods of the different models was slightly higher than the scatter obtained from repeated runs for one model, it is assumed that it is not possible to rule out one of the models, especially because the order of the models indicated by their likelihoods is different for the K^+ and the Tl^+ data. A rigid test of the putative kinetic equivalence would require the evaluation of many experiments. However, already the calculations for Table 2 kept two personal computers busy for one month.

More interesting is the ratio i_{fit}/i_{sim}. It is ~1 without Tl^+, and it decreased by ~25% in the presence of Tl^+ for most models. This reaches the magnitude of the observed current reduction by the AMFE. Actually, the question of the true model is not important for the investigations here, because all models resulted in the same Tl^+-induced reduction of open-channel current (besides the O–C–C–C–O model where the reduction was smaller, but also significant).

Because it is not possible to identify the true model, only one of them is used for the analysis of the other data (the A–O–G–C–Z model, which happens to have an insignificantly higher likelihood). Figure 8 shows the rate constants obtained at membrane potentials of +100, +80, −80, and −100 mV in 250 mM K^+ and in 20 mM Tl^+ and 230 mM K^+. The interesting finding is that the probability of being in the long-lived open state, A, decreases in all experiments in the presence of Tl^+. The probability of being in the short-lived open (O) or short-lived closed (G) states increases. This is less obvious at −80 mV, because this was a very active channel. Nevertheless, also simulations with the rate constants of this active channel showed a 14% decrease of the apparent open-channel current in the presence of Tl^+ (Table 3). Inspecting the rate constants in Fig. 8 indicates that the AMFE is caused by a strong decrease of the ratio k_{OA}/k_{OG}, which more frequently makes the channel jump back into G. Experience has shown that the fit algorithms give a more reliable estimation of ratios than of the absolute values of these rate constants, because ratios are

TABLE 2 Testing different five-state models

Five-State Model	-log(*L*)	i_{fit}/i_{sim}
Bath: 250 mM KNO_3 + 5 mM $Ca(NO_3)_2$		
$A \underset{29,900}{\overset{4800}{\rightleftharpoons}} O \underset{47,100}{\overset{32,500}{\rightleftharpoons}} G \underset{5200}{\overset{10,200}{\rightleftharpoons}} C \underset{20}{\overset{260}{\rightleftharpoons}} Z$	7,641,300 ± 10	0.99 ± 0.01
$G \underset{87,200}{\overset{7000}{\rightleftharpoons}} A \underset{28,300}{\overset{120,500}{\rightleftharpoons}} C \underset{2900}{\overset{36,500}{\rightleftharpoons}} O \underset{10}{\overset{50}{\rightleftharpoons}} Z$	7,641,616 ± 14	0.97 ± 0.00
$G \underset{12,000}{\overset{46,500}{\rightleftharpoons}} A \underset{2800}{\overset{8400}{\rightleftharpoons}} O \underset{3700}{\overset{900}{\rightleftharpoons}} C \underset{15}{\overset{2900}{\rightleftharpoons}} Z$	7,642,302 ± 663	0.98 ± 0.01
$\begin{matrix} & & O & & \\ & & 750 \uparrow\downarrow 760 & & \\ A & \underset{48,500}{\overset{4400}{\rightleftharpoons}} & G & \underset{3900}{\overset{11,600}{\rightleftharpoons}} C \underset{10}{\overset{190}{\rightleftharpoons}} Z & \end{matrix}$	7,643,552 ± 6	0.98 ± 0.01
$A \underset{1200}{\overset{100,000}{\rightleftharpoons}} G \underset{750}{\overset{15,400}{\rightleftharpoons}} C \underset{700}{\overset{30}{\rightleftharpoons}} Z \underset{2600}{\overset{13,800}{\rightleftharpoons}} O$	7,645,980 ± 612	0.99 ± 0.00
Bath: 230 mM $K(NO_3)$ + 20 mM $TlNO_3$ + 5 mM $Ca(NO_3)_2$		
$A \underset{100}{\overset{600}{\rightleftharpoons}} O \underset{112,000}{\overset{75,000}{\rightleftharpoons}} G \underset{400}{\overset{600}{\rightleftharpoons}} C \underset{20}{\overset{200}{\rightleftharpoons}} Z$	7,473,386 ± 80	0.76 ± 0.02
$G \underset{103,000}{\overset{67,300}{\rightleftharpoons}} A \underset{122,000}{\overset{9700}{\rightleftharpoons}} C \underset{1000}{\overset{1300}{\rightleftharpoons}} O \underset{20}{\overset{240}{\rightleftharpoons}} Z$	7,475,053 ± 259	0.76 ± 0.02
$G \underset{76,300}{\overset{100,000}{\rightleftharpoons}} A \underset{4500}{\overset{800}{\rightleftharpoons}} O \underset{850}{\overset{3150}{\rightleftharpoons}} C \underset{15}{\overset{230}{\rightleftharpoons}} Z$	7,474,252 ± 80	0.79 ± 0.02
$\begin{matrix} & & O & & \\ & & 2200 \uparrow\downarrow 270 & & \\ A & \underset{63,800}{\overset{89,600}{\rightleftharpoons}} & G & \underset{950}{\overset{710}{\rightleftharpoons}} C \underset{20}{\overset{280}{\rightleftharpoons}} Z & \end{matrix}$	7,473,631 ± 40	0.77 ± 0.04
$A \underset{37,900}{\overset{100,600}{\rightleftharpoons}} G \underset{20}{\overset{240}{\rightleftharpoons}} C \underset{22,300}{\overset{2000}{\rightleftharpoons}} Z \underset{250}{\overset{240}{\rightleftharpoons}} O$	7,477,061 ± 45	0.90 ± 0.02

Time series measured at +80 mV with and without Tl^+ were fitted with the models shown by means of Eqs. 4 to 6.
The solution in the pipette was always 250 mM KNO_3 + 5 mM $Ca(NO_3)_2$, that of the bath is given in the headings. The scatter resulted from the usage of different starting values for the fits (3–4 fits per model).

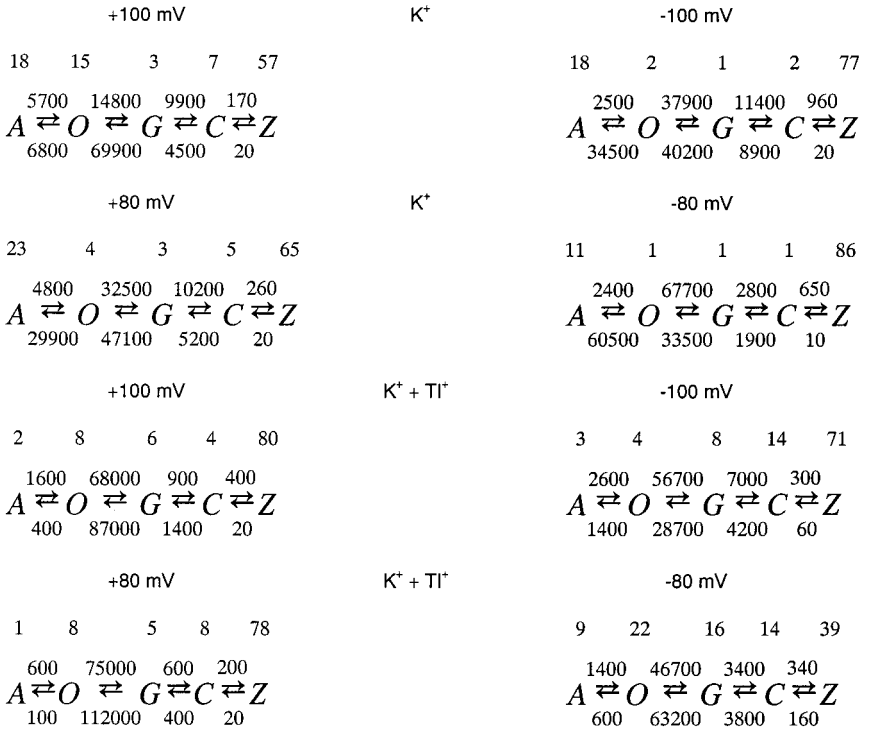

FIGURE 8 Model and single-channel rate constants (s^{-1}) obtained from direct fits of time series (20 s, $2 \cdot 10^6$ data points) at +100 and +80 mV (left-hand column) and −100 and −80 mV (right-hand column) in 250 mM KNO_3 and in 20 mM $TlNO_3$ + 230 mM KNO_3 (plus 5 mM $Ca(NO_3)_2$ in all cases). Numbers above the states give the occupation probability in percent of total time in the 20-s segment.

related to the occupation probability (in the case of A, 2–3% in the presence of Tl^+ compared to ~20% without Tl^+, Fig. 8). Occupation probabilities are usually quite exactly reproduced by fits. The experiments at positive potentials show an increase of the rate constants of the O–G exchange in the presence of Tl^+. This is less obvious at negative potentials. Thus, the lower occupation probability of A and the higher ones of O and G seem to be the major cause of faster flickering in the presence of Tl^+. This feature was not resolved by the dwell-time fits.

The dwell-times related to the data in Fig. 8 can be calculated from the k_{ij} by means of Eqs. 2 and 3 for one channel. They are shown in Table 3. The obvious feature common to all measurements is that the value of the fast time constants is not significantly changed. Instead, an ~10-fold increase of the amplitude factors of the fast com-

TABLE 3 Time constants τ (inverse eigenvalues λ) and amplitude factors d (Eq. 2) as calculated for single-channel records from the data in Fig. 8 by means of Eqs. 1–3

	K^+ +80 mV		K^+ +100 mV		$K^+ + Tl^+$ +80 mV		$K^+ + Tl^+$ +100 mV	
	d	$\tau/\mu s$	d	$\tau/\mu s$	d	$\tau/\mu s$	d	$\tau/\mu s$
A	275	800	690	560	1.4	3450	17	1170
O	5980	30	5810	84	88100	30	88500	30
G	10280	35	30680	25	149360	20	116270	20
C	145	550	240	490	3.5	3145	20	1060
Z	0.05	104030	0.04	104330	0.04	133940	0.04	118200
i_{fit}/i_{sim}	0.99		0.99		0.76		0.75	
	K^+ −80 mV		K^+ −100 mV		$K^+ + Tl^+$ −80 mV		$K^+ + Tl^+$ −100 mV	
	d	$\tau/\mu s$	d	$\tau/\mu s$	d	$\tau/\mu s$	d	$\tau/\mu s$
A	40	1530	65	1550	10	1450	33	790
O	3390	15	3180	25	25700	40	27600	35
G	2020	55	3800	35	34730	30	13700	55
C	10	835	205	265	115	500	390	560
Z	0.01	274500	0.05	113900	0.85	13730	0.45	36350
i_{fit}/i_{sim}	0.99		0.98		0.86		0.87	

The last row shows the reduction of open-channel current i_{fit}/i_{sim} in a time series simulated with the average values of the rate constants and a single-channel current i_{sim}.

ponent, d_O, of the open dwell-time histogram and of d_G of the closed dwell-time histogram is found. This means that the increased occurrence of the events with short time constants is the cause of the fast flickering, which leads to the reduction in apparent single-channel current in the presence of Tl^+.

Again, the reliability of the evaluation was tested by simulations as done in Fig. 7. Figure 9 shows that increasing rate constants used in the simulations result also in faster rate constants revealed by the fits, even though there is a lag; the fitted ones are somewhat slower than the real ones (below the $k_{fit} = k_{sim}$ line). The increasing slope in Fig. 9 is in contrast to that of the dwell-time fit. The important feature is that the data in the box are still on the ascendent branch, thus faster real rate constants would have led to faster evaluated rate constants. This provides the possibility to find the real rate constants by means of simulations, i.e., those rate constants are true that yield fitted rate constants which are identical to the fitted rate constants of the real data.

With respect to the AMFE, the most important line in Fig. 9 is the one labeled "current." It gives the apparent open-channel current obtained by evaluation of the simulated time series. The reduction of ~25% obtained from the simulated time series in Fig. 9 matches the observed reduction by the AMFE in Figs. 2 and 3. The reduction of current as obtained from simulations of this kind is given in Table 3 for all experiments. In the case of the K^+ data, the reduction in current was ~1% indicating that the reduction by fast gating is unique for the AMFE data. In the presence of Tl^+, values of 13–25% were found, which correspond to those in Figs. 2 and 3, thus showing that unresolved fast gating is probably the cause of the reduction of apparent open-channel current in the Tl^+/K^+-AMFE in *Chara*.

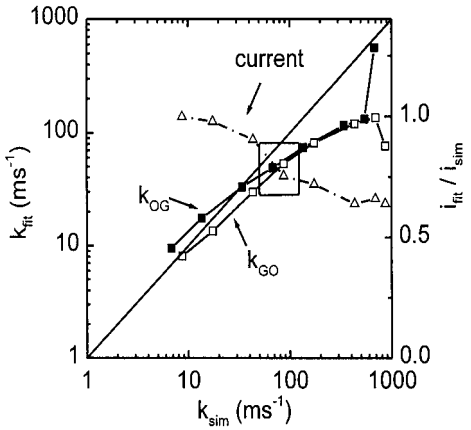

FIGURE 9 Testing the direct fit of the time series by simulated time series (k_{fit}). The rate constants evaluated from the measured time series (20 s, $2 \cdot 10^6$ data points, +100 mV, 20 mM Tl^+ + 230 mM K^+) are surrounded by the box. For the other data points, k_{GO} and k_{OG} were changed by the same factor from 0.1 to 10 (k_{sim}), whereas the other rate constants were those of the measured data. The line "current" gives the apparent open-channel current i_{fit} as determined from the simulated time series (20 s, $2 \cdot 10^6$ data points).

CONCLUSIONS

All records could be fitted with the linear five-state model shown in Fig. 8. Fit quality could not be improved by adding an extra state in the presence of Tl^+. The analysis above shows that modulation of the rate constants of fast gating is the origin of the reduction of the apparent open-channel current. The rate constants of the relevant O–G transitions are ~100 ms^{-1} (taking k_{sim} in Fig. 9 instead of k_{fit}). Together with the other rate constants (Eqs. 2 and 3), this results in a medium dwell time (inverse eigenvalue) of the open state of 30 μs (Table 3). It may be questioned whether the correct Markov model was used in Fig. 7. However, for the special purpose of the investigation here, this question is not a crucial one. Here, only a method is required that yields the reconstruction of a time series that has the same statistical properties as the measured one to study the reduction of current by gating as shown in Fig. 9. This can be done by any model that is statistically equivalent to the real model (i.e., a model that allows a direct assignment of Markov states to configurations of the channel protein).

Gating can be brought about by vibrations of the protein that open and close the channel, but also by mechanisms like those suggested by the Hille–Schwarz model (Hille and Schwarz, 1978) or the Wu model (Wu, 1991, 1992). In either case, the above analysis would provide useful information. If Tl^+-induced modifications of protein vibrations are the origin of the AMFE, the rate constants given here could be used to test the predictions obtained from molecular dynamics.

In the case of permeation models like those of Hille–Schwarz or Wu, a gap in the stream of ions can be brought about when two different ions are bound to two binding sites (Hille and Schwarz, 1978) or are involved in kicking each other from a single binding site (Wu, 1991, 1992). From the data in Fig. 8, the life times of the related states can be calculated, because the knowledge of the rate constants enables the calculation of the single-channel dwell times in the open and closed states (Table 3).

In these two models, the binding sites responsible for the AMFE would be part of the transition pathway. Because the currents in pure K^+ and pure Tl^+ are similar (Fig. 2), the rate constants of jumping from the outside into the binding site should be quite similar. Thus, it may be assumed that the probability that the "wrong" ion (that one that cannot expel the already bound one) gets in is proportional to its relative concentration. In our experiments, the chance for the wrong ion to get in would be related to 20 mM/250 mM. The average time of a jump into the binding site can be obtained from the current: 3.2 pA corresponds to 50 ns. This means that, after 0.625 μs (250 mM/20mM times 50 ns), the

stream of ions would be interrupted. This is much shorter than the average life time of the fast open state of 30 μs given in Table 3.

It should be mentioned that it is not a problem to explain the closed time (20 μs in Table 3) with the Hille–Schwarz or the Wu model. The ratio of 20 μs/50 ns would give the change in activation energy when the wrong ion has to expel the other ion out of the channel (Baukrowitz and Yellen, 1996).

There may be some errors in the above calculations of the expected open time, but it seems unlikely to assume that these errors account for a prolongation from 0.625 μs to the measured ones of 30 μs. Thus, it is concluded that models are unlikely where the AMFE-inducing binding site is part of the permeation path itself. Instead, allosteric sites on the protein are assumed that can change the rate constants of opening and closing. This explanation comes close to that suggested by Pietrobon et al. (1988) and also to the model of Draber et al. (1991).

Modification of gating frequency by such allosteric site(s) would also explain the gating in the K^+-data. In the case of the Cs^+-block, Draber and Hansen (1994) found the same number of time constants in K^+ and Cs^+/K^+ solutions. They speculated that Ca^{2+} binding (Bertl et al., 1993) was substituted by Cs^+ binding in K^+/Cs^+ solutions. However, this is not necessary. In K^+ solution, an unoccupied binding site or binding of K^+ could be the origin of the slower gating shown in Fig. 8 or Table 3.

The above questions could be settled by studying the influence of different ion concentrations on the fast gating process. However, at the moment, computers are too slow for the evaluation of hundreds of experiments, because the analysis of one experiment on a 300-MHz Pentium may take up to two weeks (3 days for one run, and different starting values have to be used for testing the convergence).

We are grateful to Dr. Thilo Riessner and to Oliver Radomski for their great support with setting up the computer programs.

REFERENCES

Albertsen, A., and U. P. Hansen. 1994. Estimation of kinetic rate constants from multi-channel recordings by a direct fit of the time series. *Biophys. J.* 67:1393–1403.

Baukrowitz, T., and G. Yellen. 1996. Use-dependent blockers and exit rate of the last ion from a multi-ion pore of a K^+ channel. *Science.* 271: 653–656.

Baum, L. E., T. Petrie, G. Soules, and N. Weiss. 1970. A maximization technique occurring in the statistical analysis of probabilistic functions of Markov chains. *Ann. Math. Statist.* 41:164–171.

Bertl, A., C. L. Slayman, and D. Gradmann. 1993. Gating and conductance in an outward-rectifying K^+ channel from the plasma membrane of *Saccharomyces cerevisiae. J. Membr. Biol.* 132:183–199.

Blunck, R., U. Kirst, T. Riessner, and U. P. Hansen. 1998. How powerful is the dwell-time analysis of multi-channel records? *J. Membr. Biol.* 165:19–35.

Chung, S. H., and P. W. Gage. 1998. Signal processing techniques for channel current analysis based on hidden Markov models. *Methods Enzymol.* 293:420–437.

Chung, S. H., J. B. Moore, L. Xia, L. S. Premkumar, and P. W. Gage. 1990. Characterization of single-channel currents using digital signal processing techniques based on hidden Markov models. *Phil. Trans. R. Soc. Lond. B.* 329:265–285.

Ciani, S., S. Krasne, S. Miyazaki, and S. Hagiwara. 1978. A model for anomalous rectification: electrochemical-potential-dependent gating of membrane channels. *J. Membr. Biol.* 44:103–134.

Colquhoun, D., A. G. Hawkes, and K. Srodzinski. 1996. Joint distributions of apparent open times and shut times of single ion channels and the maximum likelihood fitting of mechanisms. *Phil. Trans. R. Soc. Lond. A.* 354:2555–2590.

Crouzy, S. C., and F. J. Sigworth. 1990. Yet another approach to the dwell-time omission problem of single-channel analysis. *Biophys. J.* 58:731–743.

Dietrich, P., and R. Hedrich. 1998. Anions permeate and gate GCAC1, a voltage-dependent guard cell anion channel. *Plant J.* 15:479–487.

Doyle, D. A., J. M. Cabral, R. A. Pfuetzner, A. Kuo, J. M. Gulbis, S. L. Cohen, B. T. Chait, and R. MacKinnon. 1998. The structure of the potassium channel: molecular basis of K^+ conduction and selectivity. *Science.* 280:69–77.

Draber, S., and U. P. Hansen. 1994. Fast single-channel measurements resolve the blocking effect of Cs^+ on the K^+ channel. *Biophys. J.* 67:120–129.

Draber, S., and R. Schultze. 1994. Correction for missed events based on a realistic model of a detector. *Biophys. J.* 66:191–201.

Draber, S., R. Schultze, and U. P. Hansen. 1991. Patch-clamp studies on the anomalous mole fraction effect of the K^+ channel in cytoplasmic droplets of *Nitella*: an attempt to distinguish between a multi-ion single-file pore and an enzyme kinetic model with lazy state. *J. Membr. Biol.* 123:183–190.

Eisenman, G., R. Latorre, and C. Miller. 1986. Multi-ion conduction and selectivity in the high-conductance Ca^{2+}-activated K^+ channel from skeletal muscle. *Biophys. J.* 50:1025–1034.

FitzHugh, R. 1983. Statistical properties of the asymmetric random telegraph signal with application to single channel analysis. *Math. Biosci.* 64:75–89.

Fredkin, D. R., and J. A. Rice. 1992. Maximum likelihood estimation and identification directly from single-channel recordings. *Proc. Roy. Soc. Lond. B.* 249:125–132.

Friel, D. D., and R. W. Tsien. 1989. Voltage-gated calcium channels: direct observation of the anomalous mole fraction effect at the single channel level. *Proc. Natl. Acad. Sci. USA.* 86:5207–5211.

Hagiwara, S., S. Miyazaki, S. Krasne, and S. Ciani. 1977. Anomalous permeabilities of the egg cell membrane of a starfish in K^+/Tl^+ mixtures. *J. Gen. Physiol.* 70:269–281.

Hansen, U. P., A. Albertsen, C. Moldaenke, S. Draber, and R. Schultze. 1995. Detecting events in signals from sensors: the Hinkley-detector is the answer. *Sensors Materials.* 7:289–300.

Hansen, U. P., M. Keunecke, and R. Blunck. 1997. Gating and permeation models of plant channels. *J. Exp. Bot.* 48:365–382.

Hess, P., and R. W. Tsien. 1984. Mechanism of ion permeation through calcium channels. *Nature.* 309:453–456.

Hille, B., and W. Schwarz. 1978. Potassium channels as multi-ion single-file pores. *J. Gen. Physiol.* 72:409–442.

Klein, S., J. Timmer, and J. Honerkamp. 1997. Analysis of multi channel patch clamp recordings by Hidden Markov models. *Biometrics.* 53: 870–884.

Klieber, H.-G., and D. Gradmann. 1993. Enzyme kinetics of the prime K^+ channel in the tonoplast of *Chara*: selectivity and inhibition. *J. Membr. Biol.* 132:253–265.

Lühring, H. E. 1986. Recording of single channel K^+ channels in the membrane of cytoplasmic drop of *Chara australis. Protoplasma.* 133: 19–28.

Nonner, W., D. P. Chen, and B. Eisenberg. 1998. Anomalous mole fraction effect, electrostatics, and binding in ionic channels. *Biophys. J.* 74: 2327–2334.

Pallotta, B. S., and P. K. Wagoner. 1992. Voltage-dependent potassium channels since Hodgkin and Huxley. *Physiol. Rev.* 72:53–67.

Pietrobon, D., B. Prod'hom, and P. Hess. 1988. Conformational changes associated with ion permeation in L-type calcium channels. *Nature.* 333:373–376.

Press, W. H., B. P. Flannery, S. A. Teukolsky, and W. T. Vetterling. 1987. Numerical Recipes. The Art of Scientific Computing. Cambridge University Press, Cambridge, New York, New Rochelle, Melbourne, Sidney. 326–330.

Riessner, T. 1998. Level detection and extended beta distributions for the analysis of fast rate constants of Markov processes in sampled data. PhD thesis, Kiel, Germany and Shaker-Verlag, Aachen.

Roux, B., and R. Sauvé. 1985. A general solution to the time interval omission problem applied to single-channel analysis. *Biophys. J.* 48: 149–158.

Sakano, K., and M. Tazawa. 1986. Tonoplast origin of the envelope membrane of cytoplasmic droplets prepared from *Chara* internodal cells. *Protoplasma.* 131:247–249.

Schultze, R., and S. Draber. 1993. A nonlinear filter algorithm for the detection of jumps in patch-clamp data. *J. Membr. Biol.* 132:41–52.

Sigworth, F. J. 1983. Electronic design of the patch-clamp. *In* Single Channel Recording. B. Sakmann and E. Neher, E., editors. Plenum Press, New York and London. 3–35.

Tabcharani, J. A., J. M. Rommens, Y. X. Hou, X. B. Chang, L. C. Tsui, J. R. Riordan, and J. W. Hanrahan. 1993. Multi-ion pore behaviour in the CFTR chloride channel. *Nature.* 366:79–82.

Tester, M. 1988. Potassium channels in the plasmalemma of *Chara corallina* are multi-ion pores: voltage-dependent blockade by Cs^+ and anomalous permeabilities. *J. Membr. Biol.* 105:87–94.

Townsend, C., and R. Horn. 1999. Interaction between the pore and the fast gate of the cardiac sodium channel. *J. Gen. Physiol.* 113:321–331.

Wagoner, P. K., and G. S. Oxford. 1987. Cation permeation through the voltage-dependent potassium channel in the squid axon. *J. Gen. Physiol.* 90:261–290.

Wu, J. 1991. Microscopic model for selective permeation in ion channels. *Biophys. J.* 60:238–251.

Wu, J. 1992. Dynamic ion-ion and water-ion interactions in ion channels. *Biophys. J.* 61:1316–1331.

Yellen, G. 1984. Ionic permeation and blockade in Ca^{2+} activated K^+ channels of bovine chromaffin cells. *J. Gen. Physiol.* 84:157–186.

Yeo, G. F., R. K. Milne, R. O. Edeson, and B. W. Madsen. 1988. Statistical inference from single channel records: two state Markov model with limited time resolution. *Proc. R. Soc. Lond. B.* 235:63–94.